

Distribution and photo-physiological condition of phytoplankton in the tropical and subtropical North Pacific

Tetsuichi Fujiki · Kazuhiko Matsumoto ·
Toshiro Saino · Masahide Wakita · Shuichi Watanabe

Received: 29 June 2012/Revised: 4 October 2012/Accepted: 27 October 2012/Published online: 20 November 2012
© The Oceanographic Society of Japan and Springer Japan 2012

Abstract To better understand the vertical distribution of phytoplankton in the tropical and subtropical North Pacific, we used fast repetition rate fluorometry to investigate the photo-physiological condition of the phytoplankton assemblage in this region between February and March 2007. Along 155°E, between the equator and 24°N, the peak of fluorescence (F_m), an indication of the deep chlorophyll maximum (DCM), was deeper than the top of the nitracline and occurred at the 2.4 ± 1.3 % (mean \pm SD) light depth (relative to 0 m). The photochemical efficiency (F_v/F_m) and effective absorption cross-section of photosystem II (σ_{PSII}) were low at the surface but increased rapidly at depths between the top of the nitracline (40–138 m) and the DCM (70–158 m), an indication that the photo-physiological condition of the phytoplankton improved below the top of the nitracline. The depth of the maximal F_v/F_m [$Z(F_v/F_m \text{ max})$] was 18–32 m deeper than the DCM and corresponded to the 0.8 ± 0.2 % light depth. The values of F_v/F_m at the $Z(F_v/F_m \text{ max})$ were 20 % higher than those at the DCM and averaged 0.48 ± 0.01 . These results suggest that the phytoplankton assemblage beneath the DCM had a high potential photosynthetic performance capacity and was growing by using the very low ambient light in this region.

Keywords Deep chlorophyll maximum · FRR fluorometry · Photo-physiology · Phytoplankton · Tropical and subtropical North Pacific · Vertical profile

1 Introduction

The vertical distribution of phytoplankton is one of the key determinants of ecosystem structure in the ocean and hence may influence processes such as grazing, nutrient recycling, and particle sinking. In the tropical and subtropical oligotrophic oceans, the vertical distribution of phytoplankton is primarily constrained by the depth of the nitracline, and secondarily by the depth of the euphotic zone (Herbland and Voituriez 1979; Cullen 1982). Phytoplankton biomass is generally low at the surface due mostly to nutrient depletion and accumulates in a deep chlorophyll maximum (DCM) at the depth below the top of the nitracline where nutrients are sufficient to support growth (e.g., Campbell and Vaultot 1993; Babin et al. 1996). Although the DCM may not correspond exactly to the maximum of phytoplankton carbon biomass because of photoacclimation [changes in the chlorophyll (Chl) *a* content and the carbon-to-Chl *a* ratio of cells in response to variations in ambient light] (Cullen 1982), the accumulation of subsurface biomass is likely an important source of food for herbivores in the oligotrophic ocean.

Major components of the phytoplankton assemblage in oligotrophic areas include *Prochlorococcus*, *Synechococcus*, and picoeukaryotes. *Prochlorococcus* is the smallest known oxygenic photoautotroph (<1 μm) and dominates numerically throughout the euphotic zone (Partensky et al. 1999). *Synechococcus* is slightly larger than *Prochlorococcus* and is abundant, followed by *Prochlorococcus*, in oligotrophic surface waters (Marty and Chiaverini 2002;

T. Fujiki (✉) · K. Matsumoto · T. Saino · M. Wakita
Research Institute for Global Change, Japan Agency
for Marine-Earth Science and Technology,
2-15 Natsushima-cho, Yokosuka 237-0061, Japan
e-mail: tfujiki@jamstec.go.jp

M. Wakita · S. Watanabe
Mutsu Institute for Oceanography, Japan Agency
for Marine-Earth Science and Technology,
690 Kitasekine, Sekine, Mutsu 035-0022, Japan

Matsumoto et al. 2004). Picoeukaryotes often become the dominant species near the bottom of the euphotic zone, and, because they tend to be larger than prokaryotes, they contribute greatly to phytoplankton biomass (Blanchot et al. 2001). The vertical distribution of phytoplankton species is thus highly variable in the oligotrophic oceans.

An investigation of the photo-physiological condition of phytoplankton in this highly variable system should enhance understanding of their distributional characteristics. It is difficult, however, to measure variability in phytoplankton photo-physiology at small vertical (meters) scales with the use of traditional incubation-based methods such as uptake of ^{14}C or oxygen evolution. In particular, it is hard to collect phytoplankton precisely from the vicinity of the DCM, which is narrowly distributed in deep waters. To overcome this limitation, fast repetition rate (FRR) fluorometry, developed by Kolber et al. (1998), is a useful method, because FRR fluorometry can provide a rapid photo-physiological assessment without the need for time-consuming incubations and at a sufficiently high vertical resolution to detect the DCM. In addition, the fact that no bottle incubations are required eliminates artifacts associated with the enclosure of natural phytoplankton in bottles (e.g., light shock, trace metal toxicity). The utilization of FRR fluorometry in photo-physiological studies of natural phytoplankton assemblages has been documented repeatedly (e.g., Moore et al. 2006; Suggett et al. 2006; Raateoja et al. 2009).

We used FRR fluorometry in this study to investigate the vertical profile of the photo-physiological condition of phytoplankton in the vast oligotrophic North Pacific subtropical gyre, with particular attention to the DCM. We then assessed the relationship between environmental factors and the distribution and photo-physiology of the phytoplankton in this region.

2 Methods

2.1 Stations and water sampling

The observations for this study were made during the MR07-01 cruise on board R/V “Mirai” [Japan Agency for Marine-Earth Science and Technology (JAMSTEC)] in the western North Pacific Ocean from 17 February to 26 March 2007. Along 155°E, the observation interval was approximately 2° (4° for pigment measurements) from 0° to 30°N (Fig. 1). Seawater samples were collected within the upper 200 m using a bucket (surface only) and 12-L Niskin-X bottles (General Oceanics) attached to a CTD rosette system (SBE 911 plus; Sea-Bird Electronics). Nutrient concentrations were measured with an onboard TRAACS 800 system (Bran + Luebbe). We used continuous vertical

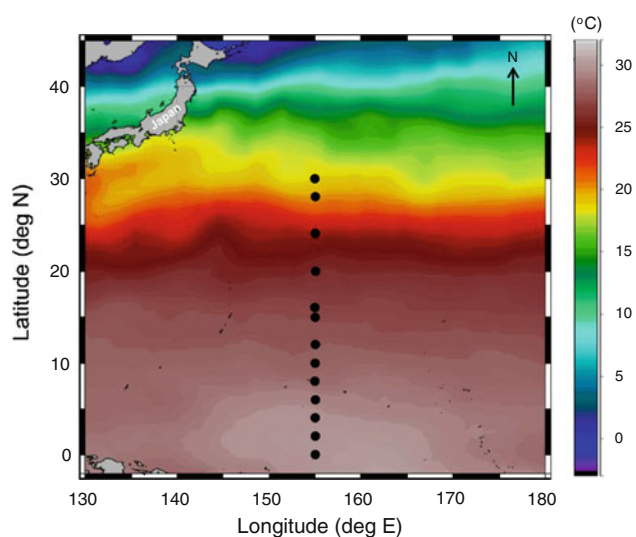


Fig. 1 Sampling locations in the western North Pacific along 155°E; colors show mean SST from 26 February to 15 March 2007 from the NGSST Development Project (courtesy of K. Sasaoka, JAMSTEC)

profiles of potential density to calculate the mixed layer depth (MLD), which we equated to the depth at which the density was 0.125 kg m^{-3} greater than the density at the surface. The depth of the top of the nitracline was derived from a cubic spline interpolation of vertical profiles of nitrate + nitrite and defined as the shallowest depth at which the rate of change of the nitrate + nitrite concentration exceeded $2 \text{ nmol kg}^{-1} \text{ m}^{-1}$ (Letelier et al. 2004).

2.2 Pigment analysis

Samples for algal pigment analysis were taken at each station from 8 depths corresponding to light levels of approximately 100, 50, 25, 10, 5, 2.5, 1, and 0.5 % relative to 0 m. These light depths were determined by using the SeaWiFS profiling multichannel radiometer and SeaWiFS multichannel surface reference sensor (Satlantic). For HPLC measurements, 5-L seawater samples were filtered onto Whatman GF/F filters (nominal pore size of $0.7 \mu\text{m}$; Whatman International) under gentle vacuum ($<0.02 \text{ MPa}$). The filters were dehydrated by freeze-drying at $-20 \text{ }^\circ\text{C}$ and then extracted with 4 mL *N,N*-dimethylformamide (DMF) for 24 h at $-20 \text{ }^\circ\text{C}$ in the dark (Suzuki and Ishimaru 1990). The extracts were filtered through $0.2\text{-}\mu\text{m}$ pore size polycarbonate filters (Millipore) to remove cellular debris and glass fibers. The filtrate was mixed with distilled-deionized water in a 7:3 volume ratio. We used the pyridine-containing mobile phase method of Zapata et al. (2000) to analyze the mixtures onboard with a HPLC system equipped with a reversed-phase C8 column (Waters). Pigment concentrations were quantified using commercially available standards (DHI Water & Environment). Because the HPLC method employed was not capable of separating monovinyl (MV) Chl *b* and divinyl (DV) Chl *b*,

we estimated the concentrations of total Chl *b* (hereafter referred as Chl *b*) with the response factor determined for MVChl *b*.

For size-fractionated Chl *a* determination, we filtered 1-L seawater samples sequentially through Nuclepore filters (Whatman International) with pore sizes of 10, 3, and 1 μm and a Whatman GF/F filter under gentle vacuum (<0.02 MPa). Each filter was extracted in DMF, and Chl *a* concentrations were measured with a fluorometer (10-AU; Turner Designs; for method, see Welschmeyer 1994). The relative Chl *a* contribution from each size fraction was expressed as a percentage of the total Chl *a* in all four fractions. Divinyl chlorophyll *a* (DVChl *a*) was included with total Chl *a* because these pigments are indistinguishable with this method.

2.3 FRR fluorometry

A custom-built FRR fluorometer was used to assess the photo-physiological condition of phytoplankton in the water column (Diving Flash; Kimoto Electric; for details, see Fujiki et al. 2008). The FRR fluorometer consisted of closed dark and open light chambers that measured the fluorescence induction curves of phytoplankton in darkness and under ambient irradiance. The dark chamber allows phytoplankton samples to dark-adapt for about 1 s before measurements to relax photochemical quenching (PQ) of fluorescence (Smyth et al. 2004). To cumulatively saturate photosystem II (PSII) within 150 μs (Kolber et al. 1998), this instrument generates a series of blue flashes (a wavelength of 470 nm with a 25-nm bandwidth) at a repetition rate of about 250 kHz and an excitation light intensity of 25 mmol quanta $\text{m}^{-2} \text{s}^{-1}$. We derived the PSII parameters from the fluorescence induction curve by using the numerical fitting procedure described by Kolber et al. (1998): these parameters included the minimum fluorescence (F_0), maximum fluorescence (F_m), and effective absorption cross-section of PSII (σ_{PSII}) in darkness, as well as the steady state fluorescence (F') and maximum fluorescence (F'_m) under ambient light. F_v is defined as ($F_m - F_0$). The F_v/F_m ratio is generally used as an index of maximum photochemical efficiency in PSII. A high value of F_v/F_m means that energy losses (as heat and fluorescence) are low, and that absorbed light energy is being efficiently utilized in photosynthesis. The σ_{PSII} is an index of the efficiency of energy transfer from the light-harvesting antenna systems to the PSII reaction centers, and the capability of the absorbed energy to promote a photochemical reaction. In this study, we determined the rate of photosynthetic electron transport per PSII reaction center [ETR, $\text{mol e}^- (\text{mol RCII})^{-1} \text{s}^{-1}$] by substituting the PSII parameters into the following equation (Gorbunov et al. 2001):

$$\text{ETR} = E \times \sigma_{\text{PSII}} \times [(F'_q/F'_m)/(F_v/F_m)] \quad (1)$$

where E is the ambient irradiance ($\mu\text{mol quanta m}^{-2} \text{s}^{-1}$) and F'_q is the change in the fluorescence measured under ambient irradiance ($= F'_m - F'$).

The FRR fluorometer together with a scalar irradiance sensor (QSP-2200; Biospherical Instruments) and a pressure gauge (ABH500PSC1B; Honeywell International) were deployed at approximately local noon from the side of the ship facing the sun. We measured vertical profiles of phytoplankton fluorescence and irradiance at intervals of approximately 1 m by lowering the instrument packages gently through the water column to a depth of 200 m and then raising them up again at a rate of 0.2 m s^{-1} . Blanks for each station were obtained by filtering seawater samples through Millipore membrane filters (pore size of 0.2 μm) (Cullen and Davis 2003). Because blank measurements could not be made vertically in the water column, the vertical fluorescence signals were corrected for background fluorescence by subtracting the fluorescence of the filtrates at 5–10 m depth from the profile values. In near-surface layers, ambient red light reaches the detector of FRR fluorometer and interferes with the fluorescence signals (red light effect) (Raateoja et al. 2004). In addition, as the FRR fluorometer shares a single photomultiplier with the detectors of dark and light chambers, the red light effect not only restricts the light chamber measurements but also influences the dark chamber measurements (Fujiki et al. 2008). In the ocean, the red light effect is confined to the upper 5–10 m (Suggett et al. 2001; Sosik and Olson 2002). Hence, for this study, we excluded data from the surface layer (about 10 m).

Midday FRR fluorometer measurements generally show low values of PSII parameters at the surface, where the incident irradiance is highest, because of non-photochemical quenching (NPQ) and photoinhibition as well as PQ (Falkowski and Raven 2007). In order to assess the potential influence of NPQ and photoinhibition, we performed measurements in a dark chamber on discrete seawater samples drawn from Niskin bottles at seven depths within the upper 200 m at 12°N on 4 March during a period of time when the daily irradiance was high (>40 mol quanta $\text{m}^{-2} \text{day}^{-1}$) for three consecutive days. On 4 March, the midday surface irradiance exceeded 1,600 $\mu\text{mol quanta m}^{-2} \text{s}^{-1}$. Before the measurements, we dark-adapted the discrete samples at in situ temperatures for 60 min.

3 Results

A composite map (satellite image analysis) of sea surface temperature (SST) from the New Generation Sea Surface Temperature (NGSST) Development Project (<http://www.>

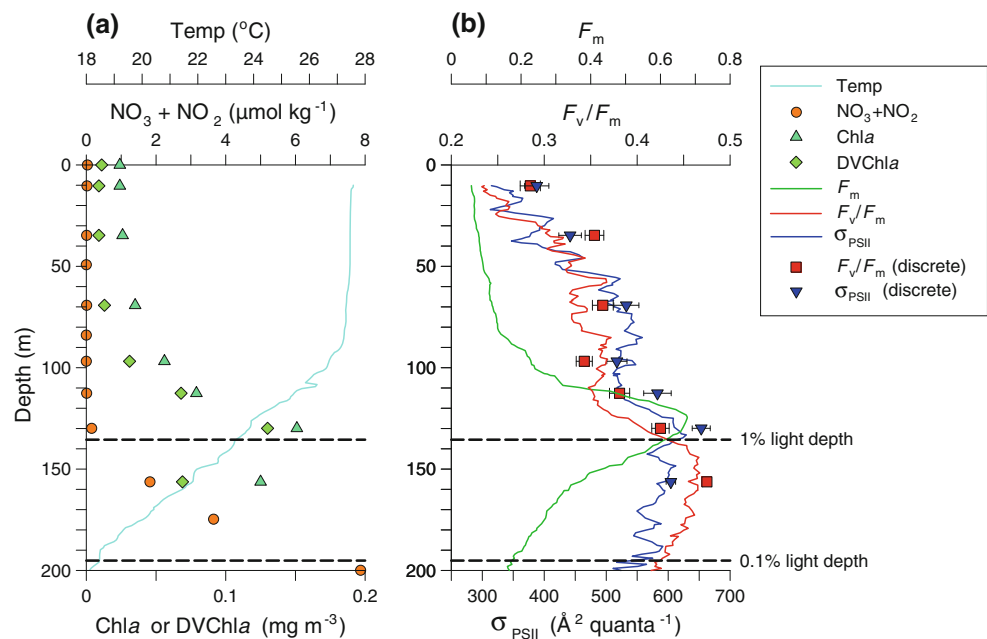
ocean.caos.tohoku.ac.jp/~merge/sstbinary/actvalbm.cgi?eng=1) showed that, during the study period, SST higher than 25.0 °C had spread as far north as roughly 25°N. In addition, the fact that SST decreased rapidly north of 30°N (Fig. 1) suggests that most of the sampling stations in this study were in the tropics and subtropics.

Typical vertical profiles of environmental variables, and Chl *a* and DVChl *a* concentrations (Fig. 2a) show that: (1) temperature was almost constant (27.4–27.6 °C) in the upper 60 m and decreased sharply with depth below 90 m; (2) concentrations of nitrate + nitrite (NO₃ + NO₂) were very low (<0.03 μmol kg⁻¹) from the surface to 110 m, but then began to increase and exceeded 2 μmol kg⁻¹ at depths >160 m; (3) concentrations of ammonium, phosphate, and silicate were <0.01 (below the detection limit), 0.10–0.71 and 0.92–6.19 μmol kg⁻¹, respectively, within the upper 200 m (data not shown); and (4) Chl *a* concentrations were <0.05 mg m⁻³ in the water column above 90 m but increased rapidly to ca 0.15 mg m⁻³ in the vicinity of 130 m, and then decreased sharply with depth. Vertical profiles of DVChl *a* and Chl *a* concentrations were similar. The continuous vertical profile of F_m values (Fig. 2b) was characterized by low values at the surface and a distinct peak at depths of 120–130 m. The DCM depth was determined from the depth of maximal F_m [$Z(F_{m \max})$] because the vertical profiles of Chl *a* and DVChl *a* were too scarce. The F_v/F_m ratio was low at the surface, increased to maximal values (0.47) about 25 m beneath the DCM, and then decreased gradually at greater depths. Although σ_{PSII} was quite variable compared to F_v/F_m , the cross-section values increased with depth and

peaked (630 Å² quanta⁻¹) near the DCM. In near-surface waters, values of F_v/F_m and σ_{PSII} from underwater measurements were lower than those from dark-adapted discrete samples (e.g., lower by 17 and 19 %, respectively, at 10 m) because of progressive NPQ and photoinhibition. At the depth below 70 m (10 % light depth), the values from underwater measurements were almost identical to those from dark-adapted discrete samples, suggesting that the influence of NPQ and photoinhibition occurred mostly in the upper 10 % light depth. However, even after we minimized the influence of NPQ and photoinhibition by the measurements of discrete samples, the maximum values of F_v/F_m and σ_{PSII} both occurred near the base of the euphotic zone.

Northward from the equator along the 155°E transect, the MLD deepened gradually to 104 m at 15°N and then shoaled again (Fig. 3). North of 28°N, increased vertical mixing due to inflow of the Kuroshio extension weakened stratification in the water column. The top of the nitracline was at or below the MLD and was deepest (138 m) at 15°N. Although the top of the nitracline deepened again at 30°N, the NO₃ + NO₂ concentration was as high as 0.42 μmol kg⁻¹, even in near-surface waters (5 m). At latitudes of 0–24°N, the $Z(F_{m \max})$, an indication of the DCM, was deeper (18–32 m) than the top of the nitracline, and was observed at the 2.4 ± 1.3 % (mean ± SD) light depth (Table 1). There was the highly significant linear relationship between F_m and NO₃ + NO₂ at the $Z(F_{m \max})$ ($r^2 = 0.74$, $n = 11$; Fig. 4). The $Z(F_v/F_m \max)$ (the depth of maximal F_v/F_m) was greater than $Z(F_{m \max})$ and corresponded to the 0.8 ± 0.2 % light depth (Table 1). Values

Fig. 2 Vertical profiles of **a** temperature, NO₃ + NO₂, HPLC-based Chl *a*, and DVChl *a* concentrations, and **b** FRR-based PSII parameters (F_m , F_v/F_m , σ_{PSII}) measured at 12°N along 155°E. In **(b)**, the values (±SE) of F_v/F_m and σ_{PSII} in discrete samples were measured after dark-adaptation for 60 min (see “Methods”). Horizontal dashed lines are the 0.1 and 1 % light depths [compared to the irradiance at 0 m (just below the surface)]



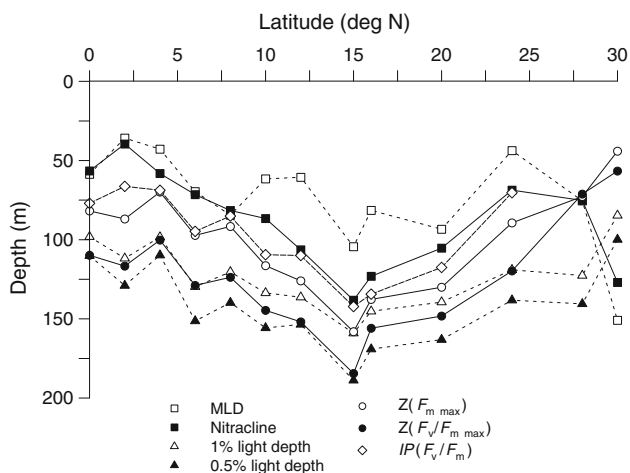


Fig. 3 Section along 155°E of the mixed layer depth (MLD), the top of the nitracline, 0.5 and 1 % light depths, $Z(F_{m \max})$, $Z(F_v/F_{m \max})$, and the inflection points of the F_v/F_m profiles ($IP(F_v/F_m)$, see “Discussion”)

of F_m at the $Z(F_v/F_{m \max})$ were less than half of those at the $Z(F_{m \max})$, but the values of F_v/F_m at $Z(F_v/F_{m \max})$ were 20 % higher than those at $Z(F_{m \max})$. There were significant differences in the all PSII parameters (F_m , F_v/F_m and σ_{PSII}) between the MLD, $Z(F_{m \max})$, and $Z(F_v/F_{m \max})$ (Kruskal–Wallis test, $p < 0.05$). The ETR ($\text{mol e}^- (\text{mol RCII})^{-1} \text{s}^{-1}$) calculated using Eq. 1 were 333 ± 182 at the MLD, 105 ± 62 at the $Z(F_{m \max})$, and 33 ± 12 at the $Z(F_v/F_{m \max})$ (Table 1).

Picoplankton ($< 3 \mu\text{m}$ diameter) dominated the total Chl a abundance at latitudes of 0–24°N, and the contribution of the $< 3 \mu\text{m}$ size fraction was consistently high ($78 \pm 8 \%$) throughout the water column (Fig. 5a). Large phytoplankton ($> 10 \mu\text{m}$ diameter) accounted for a minor fraction ($6 \pm 6 \%$) of the total Chl a . The $< 1 \mu\text{m}$ size fraction accounted for a large percentage of the picoplankton biomass in the surface waters and for $59 \pm 8 \%$ at the 50 % light depth. At the 2.5 % light depth coincident with the DCM, the $< 1 \mu\text{m}$ size fraction accounted for $50 \pm 14 \%$, followed by the 1–3 μm size fraction with $32 \pm 13 \%$. At the 1 and 0.5 % light depths [including the $Z(F_v/F_{m \max})$], the 1–3 μm size fraction increased to $41 \pm 9 \%$, a contribution that was comparable to that of the $< 1 \mu\text{m}$ size fraction ($41 \pm 12 \%$). At latitudes of 0–24°N, the major pigments detected by HPLC were 19'-butanoyloxyfucoxanthin (19'-But), fucoxanthin (Fuco), 19'-hexanoyloxyfucoxanthin (19'-Hex), zeaxanthin (Zea), Chl b , and DVChl a (Fig. 5b). The ratios of 19'-But and 19'-Hex to Chl a increased gradually with depth, whereas the ratio of Fuco to Chl a decreased with depth. The photo-protective carotenoid Zea was the dominant pigment at shallow depths. The ratio of Zea to Chl a decreased from 1.15 ± 0.22 at the surface to 0.13 ± 0.05 at the 0.5 % light depth. DVChl a , which is a unique biomarker pigment for

Table 1 Comparison of hydrographic data, PSII parameters, and photosynthetic electron transport per PSII reaction center (ETR) at three different depths [mixed layer depth (MLD), $Z(F_{m \max})$, and $Z(F_v/F_{m \max})$] along 155°E in the latitude range 0–24°N

	MLD	$F_{m \max}$	$F_v/F_{m \max}$
Depth (m)	67 ± 22	108 ± 28	135 ± 25
Temperature (°C)	27.7 ± 1.8	25.7 ± 2.1	22.7 ± 2.6
$\text{NO}_3 + \text{NO}_2$ ($\mu\text{mol kg}^{-1}$)	–	1.3 ± 1.7	4.5 ± 3.5
Relative PAR (%)	10.9 ± 7.0	2.4 ± 1.3	0.8 ± 0.2
F_m	0.21 ± 0.13	0.82 ± 0.33	0.36 ± 0.05
F_v/F_m	0.37 ± 0.03	0.40 ± 0.04	0.48 ± 0.01
σ_{PSII} ($\text{\AA}^2 \text{ quanta}^{-1}$)	529 ± 57	632 ± 37	591 ± 23
ETR ($\text{mol e}^- (\text{mol RCII})^{-1} \text{s}^{-1}$)	319 ± 168	105 ± 62	33 ± 12

The $\text{NO}_3 + \text{NO}_2$ concentrations at $Z(F_{m \max})$ and $Z(F_v/F_{m \max})$ were estimated with a cubic spline interpolation. Values listed are the mean ± 1 SD for each depth

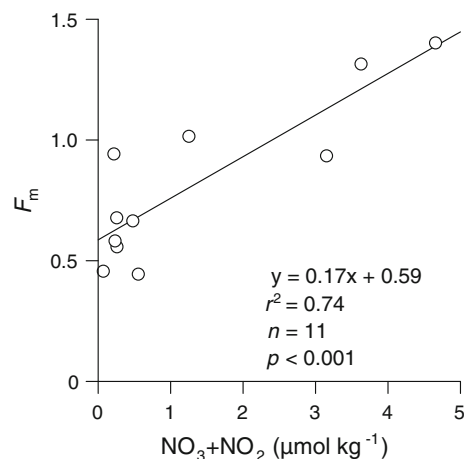
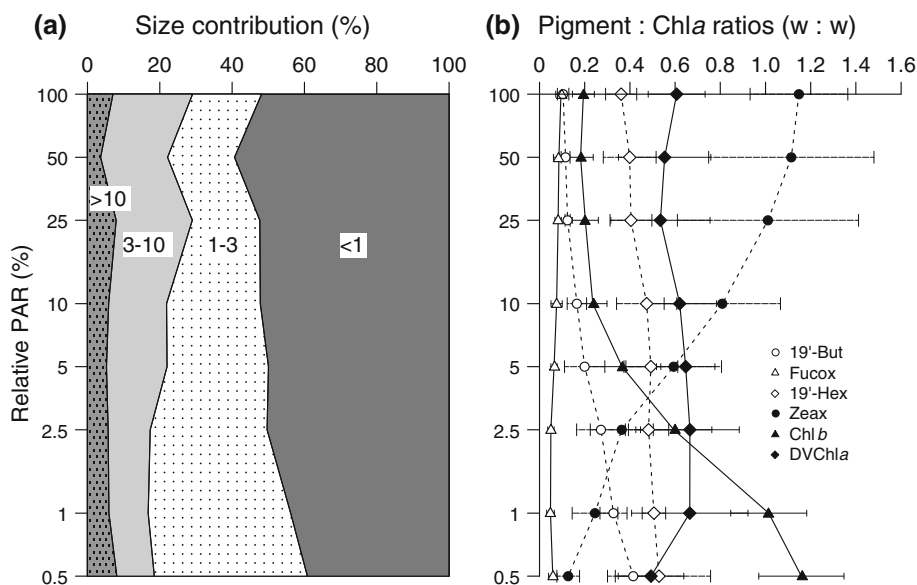


Fig. 4 Relationship between $\text{NO}_3 + \text{NO}_2$ and F_m at the $Z(F_{m \max})$, which is indicative of the DCM

Prochlorococcus, did not vary greatly relative to Chl a as a function of light depth. The relative contribution of Chl b [a biomarker pigment for green algae (chlorophytes and prasinophytes) and *Prochlorococcus*] increased with light depth, and Chl b became the most abundant photosynthetic pigment at the 0.5–1 % light depth, including the $Z(F_v/F_{m \max})$. Because the ratio of DVChl a to Chl a was almost constant within the euphotic layer, the increase in the ratio of Chl b to Chl a near the 0.5–1 % light depth may have been associated with green algae as well as *Prochlorococcus*. This hypothesis is supported by the relative increase of the 1–3 μm size fractions at the 0.5–1 % light depths (Fig. 5a), because the *Prochlorococcus* cells were $< 1 \mu\text{m}$ in diameter.

Fig. 5 Vertical distributions (as percentage of surface PAR penetration) of **a** the percentage contribution of each size fraction (<1, 1–3, 3–10, and >10 μm) to total Chl *a* and **b** the ratios of biomarker pigments (19'-But, Fuco, 19'-Hex, Zea, Chl *b*, and DVChl *a*) to Chl *a*. The values are averages for tropical and subtropical waters in the latitude range 0–24°N (4° intervals) along 155°E. Error bars in (b) $\pm 1\text{SD}$



4 Discussion

4.1 Phytoplankton assemblage around the DCM

In the oligotrophic North Pacific ocean, we observed that the $Z(F_{m \max})$, an indication of the DCM, was consistently deeper than the top of the nitracline, where the effects of nutrient limitation are diminished (Fig. 3). Moreover, the significant linear relationship between F_m and $\text{NO}_3 + \text{NO}_2$ at the DCM, as shown in Fig. 4, suggests that the magnitude of the DCM is constrained primarily by the availability of $\text{NO}_3 + \text{NO}_2$. Note, however, that the values of F_m include the fluorescence from DVChl *a* as well as Chl *a*. *Prochlorococcus* cells have been considered incapable of utilizing NO_3 and NO_2 because they lack NO_3 and NO_2 reductase activities and are known to use ammonia and urea as the source of nitrogen (Palinska et al. 2002). It was difficult to estimate only DVChl *a* fluorescence from F_m because the ratios of DVChl *a* and Chl *a* are variable over the relevant vertical and horizontal length scales (Fig. 5b). But the depth of maximal DVChl *a* was roughly comparable to that of maximal Chl *a* (Fig. 2a). Interestingly, the ammonium concentrations near the DCM were below the detection limit, although the urea concentrations were not measured in the present study. On the other hand, the incubation experiments in the Mediterranean Sea showed that NO_3 addition stimulated *Prochlorococcus* cell cycle (Vaulot and Partensky 1992), suggesting that some populations may be able to take up NO_3 . Hence, the nitrogen source used by *Prochlorococcus* near the DCM need to be examined in greater detail.

The vertical profile of F_v/F_m at 12°N showed a gradual increase in F_v/F_m with depth, the slope of increase accelerating from $4.7 \times 10^{-4} \text{ m}^{-1}$ between 60 and 110 m to

$3.8 \times 10^{-3} \text{ m}^{-1}$ between 110 and 140 m. The change in slope at 110 m occurred just below the top of the nitracline (Fig. 2). At other latitudes between 0 and 24°N, the inflection points of the F_v/F_m profiles were located between the top of the nitracline and the DCM (Fig. 3). Because F_v/F_m has been generally used as an indicator of nutrient stress (e.g., Cleveland and Perry 1987; Geider et al. 1993), these features of the F_v/F_m profiles indicate that nutrient limitation of photosynthetic performance was probably reduced near the top of the nitracline. As was the case with F_v/F_m , σ_{PSII} increased gradually with depth and displayed an inflection point below the top of the nitracline (Fig. 2). The implication is that σ_{PSII} was suppressed in the upper water column relative to below the top of the nitracline. This result is inconsistent with the conventional concept that nutrient limitation leads to an increase in σ_{PSII} because of a reduction in the cellular density of functional PSII reaction centers relative to the complement of antenna pigments (Kolber et al. 1988). However, in a nutrient-replete laboratory experiment (Fujiki et al. 2007), we showed that σ_{PSII} increased with decreasing growth irradiance, whereas F_v/F_m was almost constant. This result indicates that phytoplankton have an enhanced capability to grow at low irradiance, to absorb photons, and to transfer excitation energy to PSII reaction centers. The increase in σ_{PSII} was caused by a shift from photo-protective pigments to photosynthetic pigments (Fig. 5b) and an increase in the size of the antenna serving PSII reaction centers. In this study, therefore, the increase in σ_{PSII} below the top of nitracline may have resulted from a combination of factors: stress from nutrient limitation was reduced, and the phytoplankton assemblage could thereby acclimate to the low irradiance environment. The interpretation, in this case, is that the apparent change in σ_{PSII} reflected an increase in

σ_{PSII} due to photoacclimation that prevailed over the decrease in σ_{PSII} due to a reduction in stress from nutrient limitation. These observations suggest that improvement of the photo-physiological condition of the phytoplankton occurred below the top of the nitracline, and the increased supply of $\text{NO}_3 + \text{NO}_2$ may have promoted the formation of the DCM.

4.2 Phytoplankton assemblage below the DCM

At depths below the DCM, the relative contribution of picoeukaryotes (mainly green algae) to total Chl *a* increased, although the size-fractionated Chl *a* results (Fig. 5a) and the ratios of biomarker pigments to Chl *a* (Fig. 5b) indicate that *Prochlorococcus* was still dominant. This result is in accordance with previous work in the oligotrophic waters of the North Pacific, which has shown that picoeukaryotes become an important component in the phytoplankton assemblages near the bottom of the euphotic zone (Takahashi and Hori 1984; Campbell and Vault 1993). Ohki and Honjho (1997) isolated picoeukaryotes (<2 μm in diameter), which have a high concentration of Chl *b*, from subsurface waters in the Kuroshio area near Japan and used electron microscopy to show that a single chloroplast occupied a large part of the cytoplasm. They suggested that the high Chl *b* concentrations and the large chloroplast of the small cells enabled them to make efficient use of the reduced light in their habitat. We have no data that would enable us to determine the exact taxonomic affiliation of the phytoplankton assemblage; however, the results of our pigment analyses imply that green algae, as well as *Prochlorococcus*, were able to acclimate to very low ambient irradiance.

An interesting observation of this study is the fact that $Z(F_v/F_m \text{ max})$ (135 ± 25 m) was located below the $Z(F_m \text{ max})$ (i.e., DCM, 108 ± 28 m) (Table 1). Corno et al. (2008) observed a similar vertical distribution of $Z(F_m \text{ max})$ and $Z(F_v/F_m \text{ max})$ at Station ALOHA ($22^\circ 45' \text{N}$, $158^\circ 00' \text{E}$) in the North Pacific subtropical gyre during the period September 2002 to December 2004. They conducted FRR fluorometer measurements at night (between 0000 and 0300 hours local time) and found high F_v/F_m values at and below the DCM. The high nocturnal F_v/F_m values mean that the phytoplankton can efficiently use light energy absorbed in photochemical reactions when they are exposed to ambient light in the daytime. The implication is that phytoplankton possess a high potential photosynthetic performance capacity. However, the fact that measurements were made only during the night confound assessment of in situ photosynthetic performance during the day, especially given the absence of information on ambient irradiance and its depth of penetration. In this study, we conducted FRR fluorometer measurements at around

midday and showed that the $Z(F_v/F_m \text{ max})$ was significantly deeper than the DCM and corresponded to the 0.8 ± 0.2 % light depth (Table 1). The ETR of the phytoplankton assemblage at the $Z(F_v/F_m \text{ max})$ was as low as 33 ± 12 mol e^- (mol RCII) $^{-1}$ s^{-1} , about one-third of the ETR (105 ± 62) at the DCM, where the ambient irradiance (2.4 ± 1.3 % light depth) was three times higher (Table 1). The occurrence of the maximal F_v/F_m below the DCM could reflect a further reduction of nutrient stress of the phytoplankton assemblage as a whole and a change of species composition, as shown by the relative increase of green algae. Suggest et al. (2009) recently verified that both PSII parameters and the photo-physiological condition of phytoplankton vary across algal taxa. They showed, for example, that some species of *Synechococcus* had relatively low values of both F_v/F_m and σ_{PSII} compared to eukaryotes and *Prochlorococcus* based on experiments involving excitation with blue light flashes. Our study cannot clarify the primary factor that contributes to development of a phytoplankton assemblage deeper than the DCM with the highest F_v/F_m in the water column, but a secondary factor is the change of species composition in deeper waters that may result from differences among species in nutritional requirements for growth. The results of this study suggest that the photo-physiological condition of the phytoplankton assemblage below the DCM was not weak. Instead, the cells had a high potential photosynthetic performance capacity and were growing at a very low irradiance that was nevertheless sufficient for them to utilize the abundant nutrients in deeper waters of the tropical and subtropical North Pacific.

5 Conclusions

The vertical distribution of F_m in the oligotrophic areas that were the focus of this study is consistent with the two-layer model for the euphotic zone proposed by Dugdale (1967): a nutrient-limited phytoplankton assemblage overlies a light-limited assemblage. It is well known that nutrient-limited phytoplankton assemblages characterize the portions of the upper water column where recycled nutrients support most of the primary production, whereas new production accounts for a higher percentage of photosynthesis in the light-limited portion of the water column (Coale and Bruland 1987). The vertical gradients of PSII parameters and the composition of pigments reported here suggest that the phytoplankton assemblage in the lower euphotic zone could be further separated into two layers: an assemblage near the DCM and another assemblage beneath the DCM. Our results also appear to show that the phytoplankton assemblage near the DCM depended mainly on $\text{NO}_3 + \text{NO}_2$ as a source of nitrogen (as evidenced by the

relationship between F_m and $\text{NO}_3 + \text{NO}_2$) and that the assemblage below the DCM was constrained primarily by the low ambient irradiance (as evidenced by the low ETR). It is possible that further detailed studies will show that phytoplankton assemblages at and below the DCM may be able to grow in response primarily to an increase in nitrogen availability and ambient irradiance, respectively. In the absence of measurements of nutrient concentrations and irradiance, the difference in depth of $Z(F_{m \text{ max}})$ and $Z(F_v/F_{m \text{ max}})$ in tropical and subtropical regions may be a useful indicator of the fact that phytoplankton assemblages at and below the DCM are nutrient- and light-limited, respectively.

Acknowledgments This work was supported by the western North Pacific biogeochemical study program of the Japan Agency for Marine-Earth Science and Technology (JAMSTEC). We are grateful to the captain and crew of the R/V "Mirai" for their support during the cruise, to the staff of Marine Works Japan, Ltd. and Global Ocean Development, Inc. for their on-board analysis and deck work. We thank K. Sasaoka (JAMSTEC) for satellite data and the interpretation of these data. We are also indebted to M.C. Honda for valuable comments that improved the manuscript.

References

- Babin M, Morel A, Claustre H, Bricaud A, Kolber Z, Falkowski PG (1996) Nitrogen- and irradiance-dependent variations of the maximum quantum yield of carbon fixation in eutrophic, mesotrophic and oligotrophic marine systems. *Deep Sea Res I* 43:1241–1272
- Blanchot J, André JM, Navarette C, Neveux J, Radenac MH (2001) Picophytoplankton in the equatorial Pacific: vertical distributions in the warm pool and in the high nutrient low chlorophyll conditions. *Deep Sea Res I* 48:297–314
- Campbell L, Vault D (1993) Photosynthetic picoplankton community structure in the subtropical North Pacific Ocean near Hawaii (station ALOHA). *Deep Sea Res I* 40:2043–2060
- Cleveland JS, Perry MJ (1987) Quantum yield, relative specific absorption and fluorescence in nitrogen-limited *Chaetoceros gracilis*. *Mar Biol* 94:489–497
- Coale KH, Bruland KW (1987) Oceanic stratified euphotic zone as elucidated by ^{234}Th : ^{238}U disequilibria. *Limnol Oceanogr* 32:189–200
- Corno G, Letelier RM, Abbott MR, Karl DM (2008) Temporal and vertical variability in photosynthesis in the North Pacific Subtropical Gyre. *Limnol Oceanogr* 53:1252–1265
- Cullen JJ (1982) The deep chlorophyll maximum: comparing vertical profiles of chlorophyll *a*. *Can J Fish Aquat Sci* 39:791–803
- Cullen JJ, Davis RF (2003) The blank can make a big difference in oceanographic measurements. *Limnol Oceanogr Bull* 12:29–35
- Dugdale RC (1967) Nutrient limitation in the sea: dynamics, identification, and significance. *Limnol Oceanogr* 12:685–695
- Falkowski PG, Raven JA (2007) *Aquatic photosynthesis*, 2nd edn. Princeton University Press, New Jersey
- Fujiki T, Suzue T, Kimoto H, Saino T (2007) Photosynthetic electron transport in *Dunaliella tertiolecta* (Chlorophyceae) measured by fast repetition rate fluorometry: relation to carbon assimilation. *J Plankton Res* 29:199–208
- Fujiki T, Hosaka T, Kimoto H, Ishimaru T, Saino T (2008) In situ observation of phytoplankton productivity by an underwater profiling buoy system: use of fast repetition rate fluorometry. *Mar Ecol Prog Ser* 353:81–88
- Geider RJ, Greene RM, Kolber Z, MacIntyre HL, Falkowski PG (1993) Fluorescence assessment of the maximum quantum efficiency of photosynthesis in the western North Atlantic. *Deep Sea Res I* 40:1205–1224
- Gorbunov MY, Kolber Z, Lesser MP, Falkowski PG (2001) Photosynthesis and photoprotection in symbiotic corals. *Limnol Oceanogr* 46:75–85
- Herbland A, Voituriez B (1979) Hydrological structure-analysis for estimating the primary production in the tropical Atlantic Ocean. *J Mar Res* 37:87–101
- Kolber Z, Zehr J, Falkowski P (1988) Effects of growth irradiance and nitrogen limitation on photosynthetic energy conversion in photosystem II. *Plant Physiol* 88:923–929
- Kolber ZS, Prášil O, Falkowski PG (1998) Measurements of variable chlorophyll fluorescence using fast repetition rate techniques: defining methodology and experimental protocols. *Biochim Biophys Acta* 1367:88–106
- Letelier RM, Karl DM, Abbott MR, Bidigare RR (2004) Light driven seasonal patterns of chlorophyll and nitrate in the lower euphotic zone of the North Pacific Subtropical Gyre. *Limnol Oceanogr* 49:508–519
- Marty JC, Chiaverini J (2002) Seasonal and interannual variations in phytoplankton production at DYFAMED time-series station, northwestern Mediterranean Sea. *Deep Sea Res II* 49:2017–2030
- Matsumoto K, Furuya K, Kawano T (2004) Association of picophytoplankton distribution with ENSO events in the equatorial Pacific between 145°E and 160°W. *Deep Sea Res I* 51:1851–1871
- Moore CM, Suggett DJ, Hickman AE, Kim YN, Tweddle JF, Sharples J, Geider RJ, Holligan PM (2006) Phytoplankton photoacclimation and photoadaptation in response to environmental gradients in a shelf sea. *Limnol Oceanogr* 51:936–949
- Ohki K, Honjo S (1997) Oceanic picophytoplankton having a high abundance of chlorophyll *b* in the major light harvesting chlorophyll protein complex. *Photosynth Res* 53:121–127
- Palinska KA, Laloui W, Bédu S, Goërl SL, Castets AM, Rippka R, Tandeau de Marsac N (2002) The signal transducer P_{II} and bicarbonate acquisition in *Prochlorococcus marinus* PCC 9511, a marine cyanobacterium naturally deficient in nitrate and nitrite assimilation. *Microbiology* 148:2405–2412
- Partensky F, Hess WR, Vault D (1999) *Prochlorococcus*, a marine photosynthetic prokaryote of global significance. *Microbiol Mol Biol Rev* 63:106–127
- Raateoja M, Seppälä J, Kuosa H (2004) Bio-optical modelling of primary production in the SW Finnish coastal zone, Baltic Sea: fast repetition rate fluorometry in Case 2 waters. *Mar Ecol Prog Ser* 267:9–26
- Raateoja M, Mitchell BG, Wang H, Olivo E (2009) Effect of water column light gradient on phytoplankton fluorescence transients. *Mar Ecol Prog Ser* 376:85–101
- Smyth TJ, Pemberton KL, Aiken J, Geider RJ (2004) A methodology to determine primary production and phytoplankton photosynthetic parameters from fast repetition rate fluorometry. *J Plankton Res* 26:1337–1350
- Sosik HM, Olson RJ (2002) Phytoplankton and iron limitation of photosynthetic efficiency in the Southern Ocean during late summer. *Deep Sea Res I* 49:1195–1216
- Suggett D, Kraay G, Holligan P, Davey M, Aiken J, Geider R (2001) Assessment of photosynthesis in a spring cyanobacterial bloom by use of a fast repetition rate fluorometer. *Limnol Oceanogr* 46:802–810

- Suggett DJ, Moore CM, Marañón E, Omachi C, Varela RA, Aiken J, Holligan PM (2006) Photosynthetic electron turnover in the tropical and subtropical Atlantic Ocean. *Deep Sea Res II* 53:1573–1592
- Suggett DJ, Moore CM, Hickman AE, Geider RJ (2009) Interpretation of fast repetition rate (FRR) fluorescence: signatures of phytoplankton community structure versus physiological state. *Mar Ecol Prog Ser* 376:1–19
- Suzuki R, Ishimaru T (1990) An improved method for the determination of phytoplankton chlorophyll using *N,N*-dimethylformamide. *J Oceanogr Soc Jpn* 46:190–194
- Takahashi M, Hori T (1984) Abundance of picophytoplankton in the subsurface chlorophyll maximum layer in subtropical and tropical waters. *Mar Biol* 79:177–186
- Vaulot D, Partensky F (1992) Cell cycle distributions of prochlorophytes in the north western Mediterranean Sea. *Deep Sea Res* 39:727–742
- Welschmeyer NA (1994) Fluorometric analysis of chlorophyll *a* in the presence of chlorophyll *b* and pheopigments. *Limnol Oceanogr* 39:1985–1992
- Zapata M, Rodríguez F, Garrido JL (2000) Separation of chlorophylls and carotenoids from marine phytoplankton: a new HPLC method using a reversed phase C₈ column and pyridine-containing mobile phases. *Mar Ecol Prog Ser* 195:29–45